SYNTHESIS OF HOLMIUM ORTHOFERRITE NANOPARTICLES BY THE CO-PRECIPITATION METHOD AT HIGH TEMPERATURE

Nguyen Anh Tien[1], Truong Chi Hien[1], Bui Xuan Vuong[2,]*

[1]*Faculty of Chemistry, Ho Chi Minh City University of Education, Ho Chi Minh City 700000, Vietnam*
[2]*Faculty of Pedagogy in Natural Sciences, Sai Gon University, Ho Chi Minh City 700000, Vietnam*

Abstract

Holmium orthoferrite $HoFeO_3$ nanoparticles were synthesized by a simple co-precipitation method via the hydrolysis of Ho (III) and Fe (III) cations in boiling water with 5% aqueous ammonia solution. After annealing the precipitate at 750 and 850 °C for 1 hour, the single-phase $HoFeO_3$ product formed with particle size < 50 nm. The synthesized nanopowders are paramagnetic materials with remanent magnetization $M_r < 0.01$ emu·g^{-1}, the coercive force $H_c = 20 \div 21$ Oe, and magnetization $M_s \sim 2.73$ emu·g^{-1} at 300 K in a maximum field of 16,000 Oe.

Keywords: $HoFeO_3$; nanoparticles; magnetic properties; co-precipitation.

Introduction

Out of the vast class of multifunctional materials, orthoferrites of rare-earth elements with a perovskite structure ($RFeO_3$), including holmium orthoferrite, have garnered much attention for use in modern technologies [1-8]. Rare-earth orthoferrite nanoparticles were obtained and used in some areas, such as photocatalysts [3, 8], chemical sensors [4], solid fuel cells [7], magneto-optical devices [1], and electromagnetic equipment [6, 9]. Holmium orthoferrite with a perovskite structure ($HoFeO_3$) is a promising functional material exhibiting ferromagnetic properties and high catalytic activity [8, 10–13].

In the study [8], holmium orthoferrite nanocrystals ($HoFeO_3$) with an average size of 27–40 nm (according to the XRD results) obtained by a combustion method using glycine were used to decompose methyl orange in visible light due to its narrow energy gap ($E_g = 2.12–2.14$ eV). $HoFeO_3$ orthoferrite with a particle size of 149.30 nm (SEM), obtained by the ceramic method from the corresponding holmium and iron (III) oxides,

---

was characterized by saturation magnetization M_s = 25.5 emu.g^{-1}, remanent magnetization M_r = 4.08 emu.g^{-1}, and a very high coercive force H_c = 2659 Oe at 10 K in a maximum field of 60,000 Oe [10]. The HoFeO$_3$ obtained in this study is a magnetically hard material (H_c >> 100 Oe) [14]; it can be used for the production of electromagnets, magnetic tapes, and magnetic recording materials. However, the magnetic characteristics of this material not only depend on the nature of the compound and its crystalline structure but also depend on the size of particles, their morphology, impurity content, and the synthesis method [10, 14-18].

Various methods have been developed for the formation of nanocrystalline holmium orthoferrite (HoFeO$_3$). These methods included a mechanochemical method with a high annealing temperature (usually > 1200 °C) [10, 15], hydrothermal synthesis with a long heating time (usually 12–48 h) [11], sol-gel technology in compliance with several influencing factors [8, 12] and even the formation under the influence of gamma radiation with modern equipment [19–20].

Several studies [21–26] described the features of the formation of RFeO$_3$ orthoferrite nanoparticles (R = La, Y, Nd) and doped with metal cations (for example, Mn, Ni, Co) by a simple co-deposition method via the hydrolysis of cations in boiling water (t° > 90 °C), followed by the addition of the corresponding precipitators. This kind of strategy has been supposed to stabilize the obtained precipitate. Thus, it results in the controllable growth of crystals better than the co-precipitation at room temperature [21–22]. HoFeO$_3$ nanoparticles have not been synthesized yet by similar methods. HoFeO$_3$ was also prepared by co-precipitation, using ethanol [27]. However, ethanol is volatile, pollutant, and flammable solvent compared to water solvent. Furthermore, the water solvent is cheaper.

This study aimed to synthesize holmium orthoferrite nanoparticles with narrow values of coercive force, remanent magnetization, and a high value of saturation magnetization by co-precipitation method in the water solvent and at high temperature.

Experimental

As starting materials, we used Ho(NO$_3$)$_3$·5H$_2$O, Fe(NO$_3$)$_3$·9H$_2$O, 25% an ammonia solution with a density of d = 0.901 g.mL^{-1} (all reagents were of CP grade), and distilled water. Solutions of holmium (III) and iron (III) nitrate were prepared by dissolving the corresponding salts in distilled water at room temperature (300 K). Boiling water (400 mL) was slowly added to the equimolar mixture (50 mL) of 0.1 M Ho(NO$_3$)$_3$ and 0.1 M Fe(NO$_3$)$_3$ solutions under continuously stirring with a magnetic stirrer (4000 rpm). After addition, the mixture of salt solutions was boiled for 10 min; then, under continuous stirring with a magnetic stirrer (4000 rpm), a 5% ammonia aqueous solution was dropped appropriately as a precipitant to complete precipitation of Ho (III) and Fe (III) cations (phenolphthalein test). Continuously, the mixture solution was stirred for more than 60 min. The precipitates were collected on a vacuum filter, washed with distilled water to a pH value of ~ 7.0, and dried at room temperature to constant weight (for approximately three days). The dried precipitate was homogenized and subjected to complex thermal analysis (Labsys Evo TG–DSC 1600 °C) with a heating rate of 10 deg.min^{-1} in an atmosphere of dry air up to 1000 °C in order to establish the optimal annealing regime, providing the formation of single-phase HoFeO$_3$.

The following methods were used to comprehensively study the characteristics of the obtained nanopowders: the phase composition and crystal structure were studied by

X-ray diffraction (XRD; D8-ADVANCE diffractometer) with CuKα radiation ($\lambda = 1.540$ Å) and Raman spectrometry (Horiba XploRA ONE); qualitative and quantitative elemental composition were studied by local X-ray microanalysis (XRM; scanning electron microscope FESEM S-4800), morphology and particle size were investigated by transmission electron microscopy (TEM; JEOL-1400); the average crystal size was determined according to the Debye Scherrer equation; parameters a, b, c and unit cell volume V of the were determined using the Rietveld method, implemented in the X'pert High Score Plus 2.2b software package, saturation magnetization in the maximal field, remanent magnetization and coercive force were determined using VSM MICROSENE EV11 magnetometer.

Results and discussion

The complex thermal analysis of the $HoFeO_3$ sample obtained by the co-precipitation of holmium (III) and iron (III) hydroxides showed (Fig. 1a) that the mass loss was ~ 36.50%, which is much higher than the one (16.73%) calculated according to the reaction equation (1):

$$Ho(OH)_3 + Fe(OH)_3 \rightarrow HoFeO_3 + 3H_2O \qquad\qquad 1$$
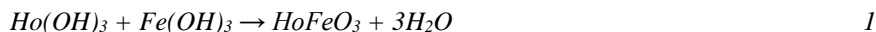
This difference is caused by the result of co-precipitation consisting not only hydroxides (($Fe_2O_3 \cdot xH_2O$ [28] and $HoO(OH) \cdot yH_2O$ [28]) but also carbonates ($Ho_2(CO_3)_3 \cdot 8H_2O$ or $Ho_2O(CO_3)_2 \cdot 1.4H_2O$) [29-30]. The presence of carbonates in the sample was probably associated with the dissolution of carbon dioxide (air) in an ammonia solution. A similar observation was reported in our previous paper for systems based on $YFeO_3$ and $LaFeO_3$ [21-22, 24, 26].
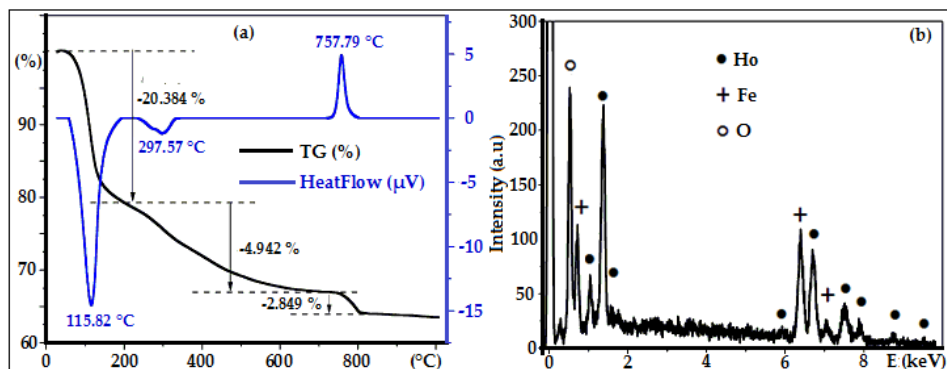

Fig. 1. TGA/DSC diagrams of the precipitate containing Ho (III) and Fe (III) (molar ratio of Ho^{3+} to Fe^{3+} is 1/1) (a), and Energy-dispersive X-ray spectroscopy (EDX) of $HoFeO_3$ nanoparticles annealed at 850 °C for 1 h (b).

The most significant mass loss (about 31.50%) observed in the range of 60–500 °C was accompanied with two endothermic peaks at 115.82 and 297.57 °C (Fig. 1a), which is assigned for water evaporation, and decomposition of holmium (III), iron (III) hydroxides. The dehydration started at 50 °C and finished at around 100 °C. On the other hand, the pyrolysis of iron (III) hydroxide and holmium hydroxide terminated at around

330 °C, 500 °C, respectively [28, 32]. Similarly, in our previous study, the pyrolysis of lanthanum hydroxide was also observed at approximately 500 °C [21].
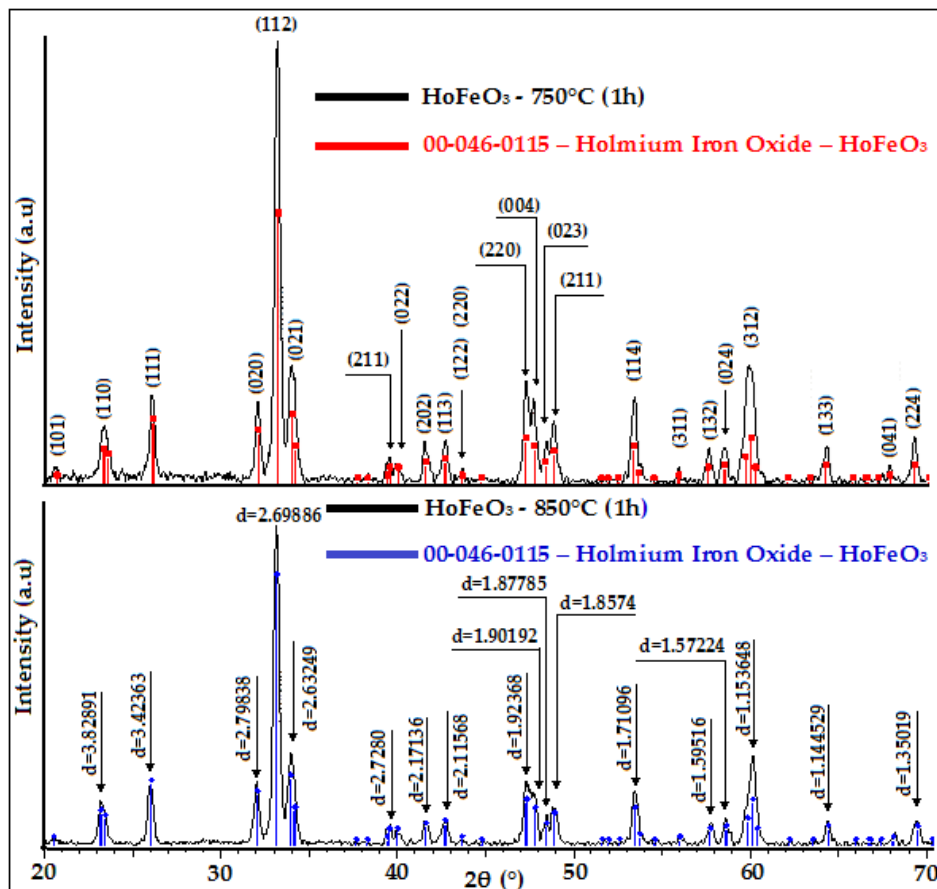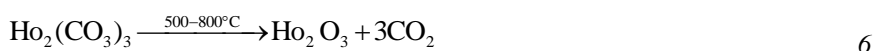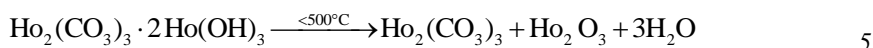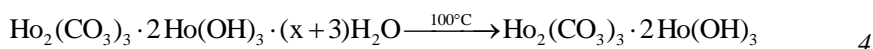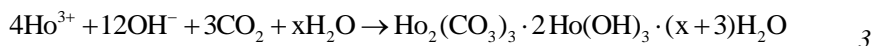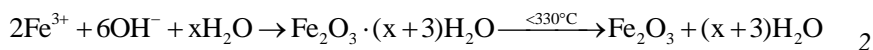

Fig. 2. XRD patterns of HoFeO₃ formed at 750 °C and 850 °C for 1 h.

The second mass loss observed in the range of 500–800 °C was related to the decomposition of holmium carbonates ($Ho_2(CO_3)_3\cdot 8H_2O$ or $Ho_2O(CO_3)_2\cdot 1.4H_2O$). We haven't observed any endothermic peak related to this phenomenon. Simultaneously, the crystallization of holmium orthoferrite nanoparticles ($HoFeO_3$) occurred at the temperature range of 750 °C – 800 °C, resulting in an obviously exothermic peak on the DSC diagram at 757 °C. Probably, the absence of an endothermic peak on the DSC thermogram in the temperature range of 500 - 800 °C corresponding to the decomposition of holmium carbonates is due to the more significant crystallization of holmium orthoferrite nanoparticles. The crystallization was confirmed by the diffraction pattern of the sample after annealing at 750 °C, which was a single-phase product, $HoFeO_3$ (Fig. 2).

Briefly, the formation of single-phase of orthoferrite holmium ($HoFeO_3$) can be described as below equations [28-30, 32].

$$2Fe^{3+} + 6OH^- + xH_2O \rightarrow Fe_2O_3 \cdot (x+3)H_2O \xrightarrow{<330°C} Fe_2O_3 + (x+3)H_2O \qquad 2$$

$$4Ho^{3+} + 12OH^- + 3CO_2 + xH_2O \rightarrow Ho_2(CO_3)_3 \cdot 2Ho(OH)_3 \cdot (x+3)H_2O \qquad 3$$

$$Ho_2(CO_3)_3 \cdot 2Ho(OH)_3 \cdot (x+3)H_2O \xrightarrow{100°C} Ho_2(CO_3)_3 \cdot 2Ho(OH)_3 \qquad 4$$

$$Ho_2(CO_3)_3 \cdot 2Ho(OH)_3 \xrightarrow{<500°C} Ho_2(CO_3)_3 + Ho_2O_3 + 3H_2O \qquad 5$$

$$Ho_2(CO_3)_3 \xrightarrow{500-800°C} Ho_2O_3 + 3CO_2 \qquad 6$$

$$Ho_2O_3 + Fe_2O_3 \xrightarrow{750-850°C} HoFeO_3 \qquad 7$$

XRD diagram indicated that synthesized samples were a single-phase product with the structure of holmium orthoferrite $HoFeO_3$ (JCPDS no. 00-046-0115, space group Pbnm (62); a = 5.282 Å, b = 5.592 Å, c = 7.608 Å) (Fig. 2). The increase in the annealing temperature led to an increase in the degree of crystallization, size of crystal particles, unit cell parameters, and a slight decrease in unit cell volume (Table 1). These results are consistent with the reported paper [27].

Table 1. Characteristics of crystalline $HoFeO_3$ nanoparticles annealed at 750, and 850 °C.for 1 h.

$HoFeO_3$	I, (a.u.)	FWHM, (°)	D, (nm)	Lattice constants, (Å)			V, (Å³)
				a	b	c	
750 °C	218.68	0.408	20.09	5.267	5.616	7.616	225.277
850 °C	238.70	0.480	23.97	5.271	5.605	7.583	224.032

Raman spectra showed 3 strong peaks at 146.8, 514.1, and 598.4 cm^{-1} (Fig. 3a). The Raman active modes of the $HoFeO_3$ were assigned based on the method recently proposed by *Gupta et al.* [31] for $RFeO_3$ (R = Tb, Dy, Ho, Er, Tm) compounds. The strongest peak at 146.8 cm^{-1} was attributed to the Ho-O vibration modes. The Raman bands above 200 cm^{-1} correspond to oxygen ions. The high-frequency mode in the $RFeO_3$ crystal may be assigned to the internal vibration related to the mutual Fe-O motion within the oxygen octahedron [20, 31], which is present in this study at wavenumbers of 514.1 and 598.4 cm^{-1}.

TEM images indicated that $HoFeO_3$ nanoparticles were uniform (if considering individual particles). The mean sizes of particles after annealing at 750 and 850 °C were 20-30 nm and 20-40 nm, respectively (Fig. 3b, 3c, and Fig. 4). The particles are strongly aggregated at higher temperatures. According to the results of local X-ray microanalysis, the $HoFeO_3$ sample contained only three elements: Ho, Fe, and O (Fig. 1b). The

calculation of the quantitative composition demonstrated that the actual content of each element was quite close to the nominal composition (Table 2).
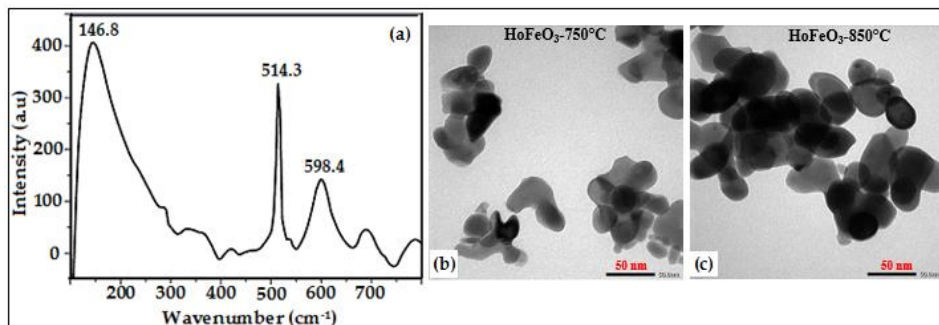

Fig. 3. Raman spectra of the HoFeO₃ nanoparticles annealed at 850 °C (a) and TEM images of the HoFeO₃ nanoparticles annealed at 750 (b) and 850 °C (c) for 1h.
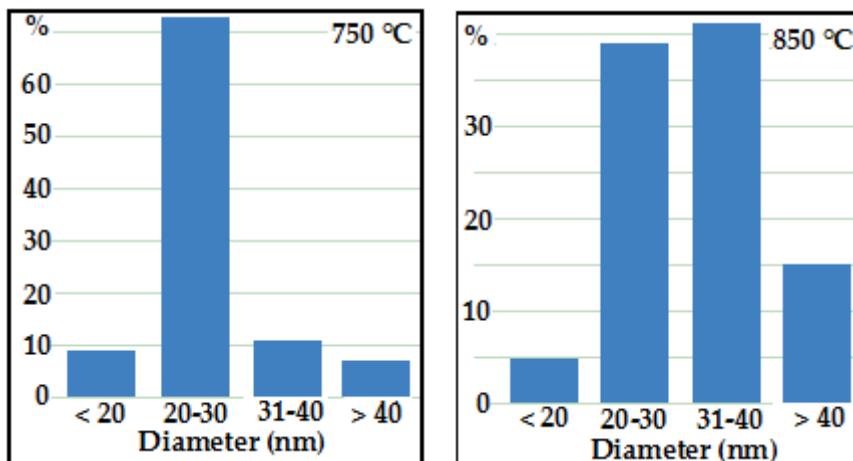

Fig. 4. Particle size distribution histogram of HoFeO₃ powders annealed at 750 and 850 °C for 1h.

Table 2. The theoretical and experimental weight percentage of Ho, Fe, and O of HoFeO₃ sample annealed at 850 °C as obtained by EDX.

Elements	Theoretical value (wt %)	Experimental value (wt %)
Ho	61.36	59.75
Fe	20.78	20.07
O	17.86	20.18

The study of the HoFeO₃ samples (annealing at 750 and 850 °C for 1 h) on a vibration magnetometer at 100 K and 300 K showed that in a maximum field of 16,000 Oe, according to the shape of the hysteresis loop, the nanopowders of HoFeO₃ are paramagnets (Fig. 5). The magnetic hysteresis curves of HoFeO₃ annealed at 750 are

similar to that of $HoFeO_3$ annealed at 850 °C. This observation is due to the same morphology (see Fig.3b-c) and insignificant changes in the crystalline size (see Table 1). Interestingly, the synthesized $HoFeO_3$ nanoparticles presented lower H_c, and M_r values $H_c \sim 20$ Oe, $M_r < 0.01$ emu/g), but higher M_s compared to the orthoferrite nanoparticles of other rare-earth elements, such as $LaFeO_3$, $YFeO_3$, and $NdFeO_3$ in similar conditions [22, 26, 32] and compared to the data of other authors for similar objects [1, 17, 33] (Table 3). Typically, the M_s value of obtained $HoFeO_3$ was much higher than that of $HoFeO_3$ prepared by the co-precipitation method using ethanol [27] (see Table 3). At 5 kOe, the magnetization of the $HoFeO_3$ sample annealed at 850 °C increases when the temperature of the measurement decreases (Fig. 5a). The $HoFeO_3$ orthoferrite samples with low coercive force, excessive magnetization, and high magnetization were investigated in this study. This material is paramagnetic and applicable in physics and biomedical, regarding quick responses to the external magnetic field [34].
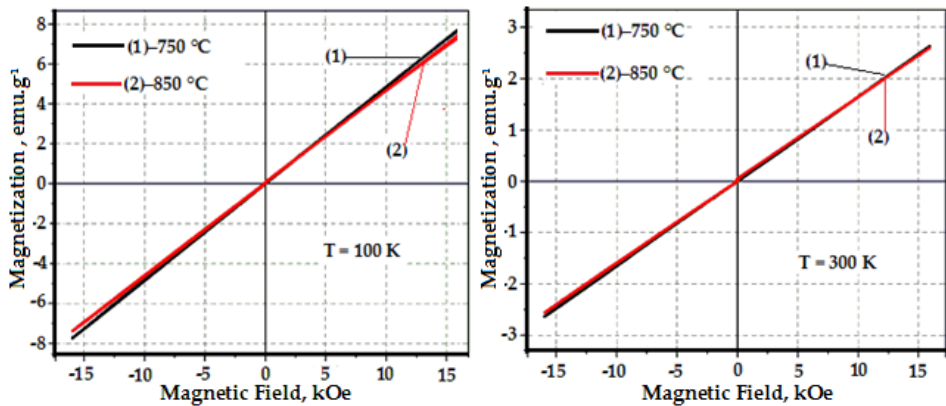

Fig. 4. Magnetization verses applied field plots of $HoFeO_3$ nanoparticles at 100 K and 300 K.

Table 3. Magnetic characteristics of $HoFeO_3$ nanoparticles in this work and those of similar nanoparticles in the published literatures, at 300 K.

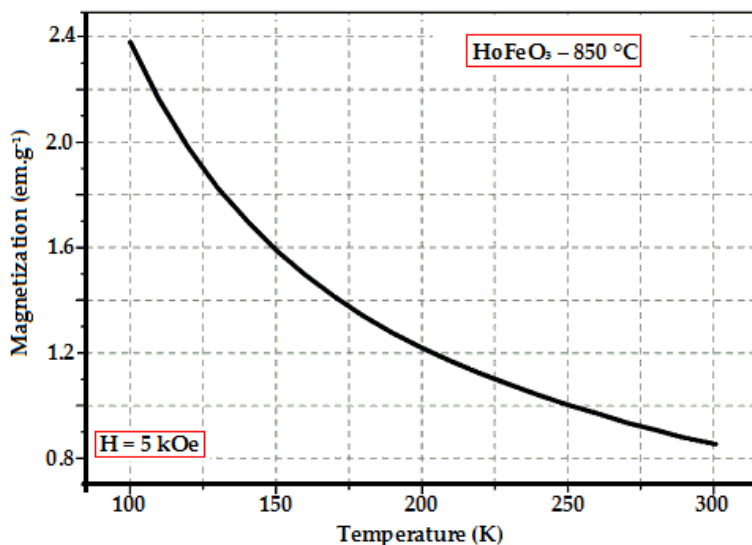| $RFeO_3$	M_r, emu/g	H_c, Oe	M_s, emu/g
$HoFeO_3$ in this work	< 0.01	20.05÷21.20	~ 2.73
$YFeO_3$, [22]	$0.19 \cdot 10^{-3}$	53.36	0.39
$LaFeO_3$, [26]	$2.00 \cdot 10^{-2}$	42.53	0.24
$NdFeO_3$, [32]	$68.0 \cdot 10^{-2}$	136.76	0.80
$HoFeO_3$, [27]	0.02÷0.04	13.95÷22.70	0.73÷0.79
$LaFeO_3$, [17]	$5.43 \cdot 10^{-4}$	1217.6	$6.49 \cdot 10^{-3}$
$LaFeO_3$, [1]	-	25-125	~ 0.10
$NdFeO_3$, [33]	1.5	~850	1.5

Fig. 5. Temperature dependence of zero-field-cold (ZFC) magnetization plot of HoFeO₃
nanoparticles annealed at 850 °C for 1h (in the presence of 5 kOe magnetic field).

Conclusions

In this study, HoFeO₃ nanoparticles were synthesized by the simple co-precipitation method via a simple process. The first stage is the hydrolysis of Ho (III) and Fe (III) cations in boiling water with an aqueous ammonia solution. The second stage is the annealing at 750 and 850 °C for 1 h. The synthesized HoFeO₃ orthoferrite nanopowders exhibited a narrow hysteresis loop, small values of remanent magnetization and coercive force, but high magnetization, which is potential use as paramagnetic material in physics and biomedical.

References

[1]   S. Phokha, S. Pinitsoontorn, S. Maensiri, S. Rujirawat: J Sol Gel Sci Tech, 71 (2014) 333-341.
[2]   M. Yousefi, S. S. Zeid, M. K. Motlagh: Curr Chem Lett, 7 (2017) 23-30.
[3]   P. Tang, X. Xie, H. Chen, Lv. Chunyan, Y. Ding: Ferr, 546 (2019) 181-187.
[4]   J. W. Fergus: Sens. Act. B Chem, 123 (2007) 1169-1179.
[5]   M. Abdellahi, A. S. Abhari, M. Bahmanpour: Cer Int, 42 (2016) 4637-4641.
[6]   Sh. Nishiyama, I. Asako, Y. Iwadate, T. Hattori: Op J Inor Chem, 5 (2015) 7-11.
[7]   O. Pekinchak, L. Vasylechko, I. Lutsyuk, Y. Vakhula, Y. Prots, W. Carrillo-Cabrera: Nano Res Lett, 11 (2016) 11:75.
[8]   I. S. Kondrashkova, K. D. Martinson, N. V. Zakharova, V. I. Popkov: Rus J Gen Chem, 88 (2018) 2465-2471.
[9]   A. Panchwanee, V. R. Reddy, A. Gupta: J Phys Conf S, 755 (2016) 012033.
[10]   Z. Habib, K. Majid, M. Ikram, Kh. Sultan: App Phys A Mater Sci Proc, 122 (2016) 550.
[11]   Zh. Zhou, L. Guo, H. Yang, Q. Liu, F. Ye: J All Compd, 583 (2014) 21-31.

[12]   L. Jiang, W. Liu, A. Wu, J. Xu, Q. Liu, G. Qian, H. Zhang: Cer Int, 38 (2012) 3667-3672.
[13]   M. Shao, Sh. Cao, Y. Wang, Sh. Yuan, B. Kang, J. Zhang, A. Wu, J. Xu: J Cryst Gr, 318 (2011) 947-950.
[14]   A. A. Rempel: Rus Chem Rev, 76 (2007) 435-461.
[15]   Zh.-Qi. Wang, Ya.-Sh. Lan, Zh.-Yi. Zeng, X-R. Chen, Q-.F. Chen: Sol St Comm, 288 (2019) 10-17.
[16]   T. Nishimura, S. Hosokawa, Y. Masuda, K. Wada, M. Inoue: J Sol Chem, 197 (2013) 402-407.
[17]   C. Sasikala, N. Durairaj, I. Baskaran, B. Sathyaseelan, M. Henini: J All Compd, 712 (2017) 870-877.
[18]   Y. J. Wu, J. Zhang, X. K. Chen, X. J. Chen: Sol St Comm, 151 (2011) 1936-1940.
[19]   M. Bhat, B. Kaur, R. Kumar, P. A. Joy, S. D. Kulkarni, K. K. Bamzai, P. N. Rotru, B. M. Wanklyn: Nucl Instr Meth Phys Res B, 243 (2006) 134-142.
[20]   Z. Habib, M. Ikram, K. Majid: Appl Phys A. Mater Sci Proc, 116 (2014) 1327-1335.
[21]   A. T. Nguyen, I. Ya. Mittova, O. V. Almjasheva, S. A. Kirillova, V. V. Gusarov: Gl Phys Chem, 34 (2008) 756-761
[22]   A. T. Nguyen, O. V. Almjasheva, I. Ya. Mittova, O. V. Stognei, S. A. Soldatenko: Inor Mater, 45 (2009) 1304-1308.
[23]   T. A. Nguyen, M. V. Berezhnaya, Th. L. Pham, V. O. Mittova, M. Q. Vo, L. T. Tr. Nguyen, H. Tr. Do, I. Ya. Mittova, E. L. Viryutina: Rus J App Chem, 92 (2019) 498-504.
[24]   A. T. Nguyen, H. D. Chau, T. Tr. L. Nguyen, V. O. Mittova, Tr. H. Do, I. Ya. Mittova: Nanosyst Phys Chem Math, 9 (2018) 424-429.
[25]   A. T. Nguyen, V. N. T. Pham, T. Tr. L. Nguyen, V. O. Mittova, Q. M. Vo, M. V. Berezhnaya, I. Ya. Mittova, Tr. H. Do, H. D. Chau: Sol St Sci, 96 (2019) 105922.
[26]   T. A. Nguyen, V. N. T. Pham, H. T. Le, D. H. Chau, V. O. Mittova, L. T. Tr. Nguyen, D. A. Dinh, T. V. Hao, I. Ya. Mittova: Cer Int, 45 (2019) 21768-21772.
[27]   T. A. Nguyen, L. T. Tr. Nguyen, V. X. Bui, D. H. T. Nguyen, H. D. Lieu, L. M. T. Le, V. Pham: J All Compd, 834 (2020) 155098.
[28]   A. G. Belous, E. V. Pashkova, V. A. Elshanskii, V. P. Ivanitskii: Inor Mater, 36 (2000) 343–351.
[29]   N. Imanaka, Physical and Chemical Properties of Rare Earth Oxides, Binary Rare Earth Oxides, Kluwer Academic Publishers, (2004) 111–113.
[30]   N. Kozo, H. Wakita, A. Mochizuki: Bull. Chem. Soc. Japan., 46 (1973) 152–156.
[31]   H. C. Gupta, M. K. Singh, L. M. Tiwari: J Ram Spectr, 33 (2002) 67-70.
[32]   T. A. Nguyen, V. Pham, Th. L. Pham, L. T. Tr. Nguyen, I. Ya. Mittova, V. O. Mittova, L. N. Vo, B. Tr. T. Nguyen, V. X. Bui, E. L. Viryutina: Cryst, 10 (2020) 219.
[33]   P. R. Babu, R. Babu: Inter J Chem Tech Res, 9 (2016) 364-369.
[34]   B. D. Cullity, C. D. Graham, Introduction to magnetic materials, 2nd ed., Wiley, A John Wiley & Sons, Inc., Publication, Canada, (2009) ISBN 978-0-471-47741-9.